IEEE Access
Multidisciplinary | Rapid Review | Open Access Journal

Received 4 September 2023, accepted 29 October 2023, date of publication 8 November 2023,
date of current version 14 November 2023.

Digital Object Identifier 10.1109/ACCESS.2023.3330947

RESEARCH ARTICLE

Theoretical and Experimental Analysis of Reversed Uneven Power Splitting Technique in GaN MMIC Doherty Power Amplifiers

CHEOL HO KIM[1] AND HYEON-JUNE KIM[2], (Life Member, IEEE)
[1]Superintelligence Creative Research Laboratory, Electronics and Telecommunications Research Institute, Daejeon 34129, South Korea
[2]Department of Semiconductor Engineering, Seoul National University of Science and Technology, Seoul 01811, South Korea

Corresponding author: Hyeon-June Kim (hyeonjunekkim@seoultech.ac.kr)

This work was supported in part by the National Research and Development Program through the National Research Foundation of Korea (NRF), Ministry of Science and ICT, under Grant 2022M3H4A1A02076394; and in part by the Institute for Information and Communications Technology Promotion (IITP) through the Korean Government (MSIP) through the Development on 28GHz Band RF Front-End for 5G Mobile Communication Terminal under Grant B0717-16-0030.

ABSTRACT We present a theoretical and experimental analysis of the use of a reversed uneven power splitting (RUPS) technique for asymmetric Doherty power amplifiers (PAs). The RUPS technique utilizes an uneven power splitter that drives more input power into the carrier amplifier, enabling shallow class-C operation of the peaking amplifier. Although the RUPS technique has played a significant role in achieving high-performance Doherty PAs, there has been a lack of comprehensive research examining the fundamental factors that contribute to its effectiveness. We conducted numerical and experimental investigations to demonstrate that the RUPS Doherty PA exhibits significant improvements in efficiency, gain, and linearity compared to conventional Doherty PAs with even power splitting (EPS). For the experiments, the EPS and RUPS networks were developed using lumped-element directional couplers. The fabricated RUPS Doherty PA, based on a 0.25-μm GaN HEMT monolithic microwave integrated circuit (MMIC) process, achieves superior overall performance at 2.14 GHz compared to the conventional EPS Doherty PA, without requiring any additional circuitry. The results verify that the RUPS technique can enhance the performance of asymmetric Doherty PAs.

INDEX TERMS Doherty power amplifier (Doherty PA), input power splitting, directional coupler, gallium nitride (GaN), monolithic microwave integrated circuit (MMIC), long-term evolution (LTE).

I. INTRODUCTION

The efficiency and linearity of power amplifiers (PAs) are typically in a trade-off relationship [1], [2], prompting PA designers to invest considerable effort in achieving optimal performance. In current wireless communication systems based on wideband code-division multiple access or orthogonal frequency division multiplexing, high peak-to-average power ratios (PAPRs) exceeding 6 dB are common [2], [3], [4], [5], [6], [7]. As a result, PAs need to maintain high efficiency at output powers significantly lower than their peak power, while still ensuring sufficient linearity. Among the various linear PA architectures for high efficiency, the Doherty PA has demonstrated outstanding performance and is widely utilized in base stations [1], [2], [3], [4], [5], [6], [7], [8], [9], [10]. The Doherty PA, consisting of a pair of amplifiers, achieves excellent efficiencies at backed-off output powers due to its active load modulation and exhibits good linearity [11], [12].

An ideal Doherty PA consists of two symmetric (equal-sized) amplifiers that operate in class-B modes (referred to as B-B Doherty PA), with the peaking amplifier precisely turning on at the breakpoint [11]. However, in practical Doherty PAs, as illustrated in Figure 1, the peaking amplifier operates in class-C mode to maintain an off-state in the low-power region, while the carrier ampli-

The associate editor coordinating the review of this manuscript and approving it for publication was Tae Wook Kim.

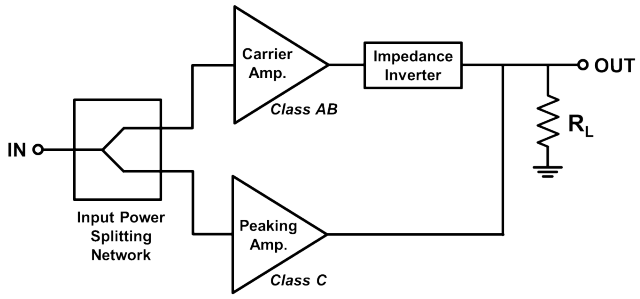

FIGURE 1. The basic AB-C Doherty configuration.

fier operates in class-AB mode to improve overall linearity. When the input power is evenly split between both amplifiers, the basic configuration leads to inadequate load modulation due to insufficient current in the class-C peaking amplifier [13]. To address this issue without the need for additional circuitry, two effective methods have been demonstrated: the asymmetric structure [13], [14], [15], [16], [17], [18] and uneven power splitting (UPS) [18], [19], [20].

The asymmetric structure was developed to expand the high-efficiency region of the Doherty PA by designing the peaking amplifier with a larger device periphery compared to the carrier amplifier [13]. The increased current in the enlarged peaking amplifier facilitated proper load modulation and further enhanced linearity through effective cancellation of third-order transconductance.

A conventional UPS [18] delivers more input power into the peaking amplifier, thereby improving linearity through proper load modulation. However, the attenuated input power towards the carrier amplifier adversely affects the gain and efficiency in the low-power region below the breakpoint where the peaking amplifier begins to activate. Adaptive UPS methods [19], [20] have been implemented to address this issue, aiming to drive more power into the carrier amplifier in the low-power region while directing more power into the peaking amplifier in the high-power region. Although these adaptive methods have achieved improved linearity and enhanced peak efficiency [19] or reduced size [20], they also have limitations, such as marginal improvements in efficiency at back-off powers and a reduction in operation bandwidth.

The reversed uneven power splitting (RUPS) technique, which delivers more power to the carrier amplifier, was first introduced in [21] and has played a significant role in achieving high-performance Doherty PAs on GaN monolithic microwave integrated circuits (MMICs) [21], [22], [23] and a printed circuit board [6]. However, a comprehensive investigation into the fundamental factors contributing to the effectiveness of RUPS has not been conducted.

In this paper, we investigate how the RUPS technique contributes to performance enhancement through theoretical analysis and experimental demonstration. Our results verify that the RUPS Doherty PA outperforms conventional even power splitting (EPS) Doherty PAs in terms of efficiency, gain, and linearity. This improvement is attributed to several factors, including increased input power in the low-power region, shallow class-C operation of the peaking amplifier, and enhanced overall output power. Furthermore, the RUPS technique can be easily implemented without the need for additional circuitry, making it applicable not only to MMIC Doherty PAs but also to generic asymmetric Doherty PAs.

The remainder of this paper is organized as follows: Section II provides a description of the conventional EPS and UPS methods, including their limitations, and presents a theoretical investigation of the RUPS method, examining its effectiveness in terms of efficiency, gain, and linearity of the Doherty PA. In Section III, we design two different lumped-element directional couplers to realize the EPS and RUPS networks. For the design of Doherty PAs utilizing these couplers, we employ GaN MMIC-based Doherty PAs, which have demonstrated notable efficiencies at back-off output powers and exhibit strong potential as small-cell base-station PAs [1], [2], [4], [5], [8], [10], [14], [21], [22], [24]. Section IV presents the results of experimental analyses, comparing the performance of the RUPS Doherty PA with that of the EPS Doherty PAs. Finally, Section V provides the conclusions of our study.

II. INPUT POWER SPLITTING OF DOHERTY PAS

The input power splitting methods for Doherty PAs can be categorized based on power splitting ratios: even and uneven ratios. In this section, we first review the conventional EPS and UPS methods. Then, we introduce the RUPS strategy and investigate its effectiveness in enhancing the performance of the Doherty PA.

A. CONVENTIONAL EVEN POWER SPLITTING (EPS) AND UNEVEN POWER SPLITTING (UPS) METHODS

The EPS method demonstrates proper load modulation in an ideal B-B Doherty PA scenario [11]. However, as mentioned in the previous section, load modulation loses its balance in the AB-C Doherty PA configuration due to inadequate output current from the peaking amplifier caused by a reduced conduction angle of class-C operation [13]. Nevertheless, the EPS approach has proven to be a valuable power-splitting technique for both symmetric and asymmetric GaN MMIC Doherty PAs [5], [8], [9], [10], [15], particularly when design simplicity in the input network or broadband performance is required.

The UPS technique, which involves supplying more input power to the peaking amplifier, restores proper load modulation, resulting in improved linearity and drain efficiency (DE) in the high-power region [18]. However, as a significant portion of the input power is delivered to the 'off-state' peaking amplifier below the breakpoint, the UPS Doherty PA experiences a reduction in gain and a consequent decrease in power-added efficiency (PAE) in the low-power region. Additionally, to prevent early turn-on caused by the increased portion of input power in the low-power region, the peaking amplifier must operate in a deeper class-C mode compared to the EPS case. This deeper class-C operation inevitably leads to a decrease in the fundamental output current and

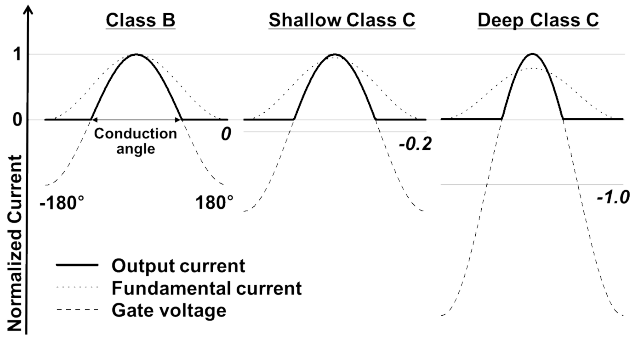

FIGURE 2. Output current waveforms of the power amplifier with different gate bias voltages.

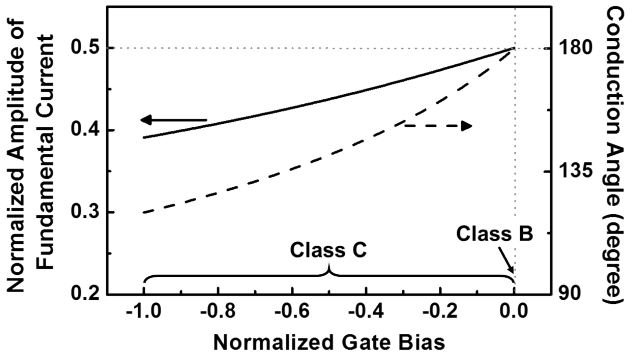

FIGURE 3. Fundamental output current and conduction angle of class-B and class-C power amplifiers as a function of normalized gate bias.

an increase in harmonic components, which deteriorate gain and linearity [11]. Furthermore, in the case of an asymmetric Doherty configuration, the UPS may achieve only marginal or minimal improvement since the asymmetry alone can provide proper modulation.

B. THE REVERSED UNEVEN POWER SPLITTING (RUPS) METHOD

To overcome the limitations of conventional power splitting techniques, we have introduced the RUPS method [21], which delivers more input power to the carrier amplifier across the entire power range. The RUPS strategy can enhance gain and PAE in the low-power region compared to the EPS technique because a significant portion of the input power is supplied to the carrier amplifier, which operates independently below the breakpoint. However, above the breakpoint, it becomes apparent that the peaking amplifier cannot deliver sufficient output current for proper load modulation due to the inadequate input power.

To compensate for the shortage of output current, we have made modifications to the peaking amplifier in two ways: by enlarging its device periphery and increasing the gate bias voltage. As mentioned earlier, in the asymmetric Doherty configuration where the peaking amplifier has a larger device periphery than the carrier amplifier, load modulation is improved due to the enhanced output current of the peaking amplifier [13]. Furthermore, the output current can be further enhanced by increasing the gate bias voltage. In the RUPS strategy, the power delivered to the peaking amplifier is smaller than that delivered to the carrier amplifier. This causes the peaking amplifier to activate at a higher input power. Consequently, we have a significant margin to increase the gate bias voltage, enabling the peaking amplifier to operate in a much shallower class-C mode compared to the EPS case.

Figure 2 illustrates the alterations in the output current waveforms of a PA for various gate bias voltages under the condition that the current peaks are kept the same. The gate voltage waveforms are normalized to the waveform for class-B mode and overlapped with dashed lines, positioning their peaks at the output current peaks. Each gate bias voltage is indicated in italic type. It is evident that the shallower class-C mode exhibits a larger conduction angle and a greater fundamental current component compared to the deeper class-C mode.

Figure 3 displays the changes in the fundamental component and conduction angle in class-C modes as a function of the normalized gate bias voltage while maintaining the peak output current. As the class-C peaking amplifier becomes shallower by increasing the gate bias, the fundamental current component is enhanced due to the increased conduction angle. For example, a shallow class-C PA with a gate bias of -0.2 improves by 20.5% compared to a deep class-C PA with a gate bias of -1.0.

The RUPS method can also enhance efficiency near the breakpoint in the high-power region. Supplying less input power to the peaking amplifier enables driving additional power even after the carrier amplifier reaches its peak current, resulting in an extension of the back-off region. Thus, we can fully leverage the peaking amplifier similar to the EPS method. Assuming the same back-off range, the peaking amplifier operating with a shallow class-C mode can achieve an efficiency advantage compared to a deep class-C mode after the breakpoint. This is due to the fact that a shallow class-C amplifier exhibits higher efficiency than a deep class-C amplifier at back-off power [25]. On the other hand, the efficiency improvement will decrease as we move towards peak power because the shallow class-C amplifier becomes less efficient than the deep class-C amplifier under full drive [25]. Nevertheless, the efficiency enhancement near the breakpoint is meaningful because the modulation signal mainly operates around the back-off power.

Of course, the additional input drive inevitably results in early current saturation of the carrier amplifier. However, its fundamental component will continue to grow to some extent, and this behavior can be readily verified through Fourier series analysis, as described in the following analysis. Furthermore, the concern of current saturation can be mitigated by slightly increasing the size of the carrier device and adjusting the input matching network to ensure proper operation at the breakpoint. This approach effectively

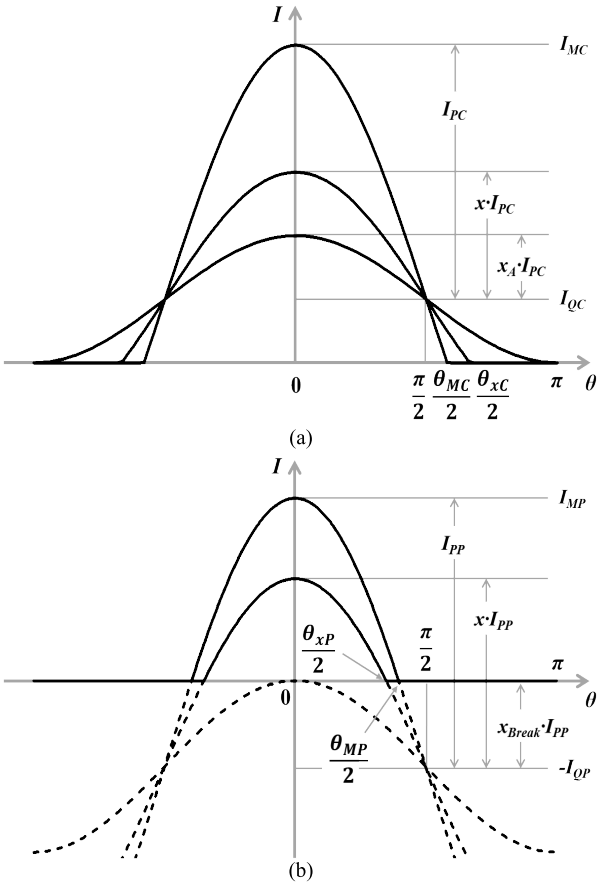

FIGURE 4. Output current waveforms for (a) the class-AB carrier amplifier and (b) the class-C peaking amplifier.

delays saturation, enabling a normal operation of the RUPS Doherty PA.

C. NUMERICAL ANALYSIS WITH AB-C DOHERTY PA MODEL

To quantitatively investigate the effectiveness of the RUPS method, we constructed an AB-C Doherty PA model [11], which is more suitable for representing a practical Doherty PA than the simple B-B model. By assuming a purely sinusoidal drive and constant transconductance, we are able to generate the output current waveforms of both amplifiers, as shown in Figure 4.

The evolution of the output current can be described by introducing a parameter x ($0 \leq x \leq x_{max}$, where x_{max} is typically 1), which is proportional to the input drive. We then define several variables to represent the waveform of the carrier amplifier as follows:

I_{QC} : quiescent current
I_{MC} : maximum current
I_{PC} : peak current amplitude at the maximum current
θ_{xC} : conduction angle
x_A : a point where the waveform starts to get truncated.

Now we represent the current waveform as follows:

$$I_C(\theta, x) = \begin{cases} I_{PC} \cdot x \cdot \cos\theta + I_{QC} \ , & -\frac{\theta_{xC}}{2} < \theta < \frac{\theta_{xC}}{2} \\ 0 & \text{otherwise} \end{cases} \quad (1)$$

where

$$I_{PC} = I_{MC} - I_{QC}$$
$$\theta_{xC}(x) = \begin{cases} 2\pi & , \quad 0 \leq x < x_A \\ 2 \cdot \cos^{-1}\left(-\frac{x_A}{x}\right) & , \ x_A \leq x \leq x_{max} \end{cases}$$
$$x_A = \frac{I_{QC}}{I_{MC} - I_{QC}}.$$

Through Fourier series expansion, we obtain the fundamental and DC components of the output waveform:

$$I_{C1}(x) = \frac{1}{\pi}\int_{-\pi}^{\pi} I_C(\theta, x) \cdot \cos\theta \cdot d\theta \quad (2)$$
$$I_{C0}(x) = \frac{1}{2\pi}\int_{-\pi}^{\pi} I_C(\theta, x) \cdot d\theta. \quad (3)$$

Similarly, we can extract the fundamental and DC components from the class-C waveform of the peaking amplifier.

I_{QP} : absolute value of virtual quiescent current
I_{MP} : maximum current
I_{PP} : peak current amplitude at the maximum current
θ_{xP} : conduction angle
x_{break} : a point where the peaking amplifier turns on (breakpoint)

We represent the current waveform for $x \geq x_{break}$ as follows:

$$I_P(\theta, x) = \begin{cases} I_{PP} \cdot x \cdot \cos\theta - I_{QP} \ , & -\frac{\theta_{xP}}{2} < \theta < \frac{\theta_{xP}}{2} \\ 0 & \text{otherwise} \end{cases} \quad (4)$$

where

$$I_{PP} = I_{MP} + I_{QP}$$
$$\theta_{xP}(x) = 2 \cdot \cos^{-1}\left(\frac{x_{break}}{x}\right).$$
$$x_{break} = \frac{I_{QP}}{I_{PP}}.$$

The fundamental and DC components of the output waveform are as follows:

$$I_{P1}(x) = \frac{1}{\pi}\int_{-\pi}^{\pi} I_P(\theta, x) \cdot \cos\theta \cdot d\theta \quad (5)$$
$$I_{P0}(x) = \frac{1}{2\pi}\int_{-\pi}^{\pi} I_P(\theta, x) \cdot d\theta. \quad (6)$$

We can express the equations in a more concise format using normalized currents: $I_{MC} = 1$ and $I_{MP} = \gamma$ where $\gamma = I_{MP}/I_{MC}$ is the maximum current ratio between the carrier and peaking amplifiers. The normalized equations are summarized in Table 1.

Since both amplifiers operate as current sources with the described current waveforms, we can construct two different equivalent circuit models separated by the breakpoint, as shown in Figure 5. In a lossless quarter-wave transmission line, the product of voltage and current is preserved, as follows:

$$V_{C1} \cdot I_{C1} = V_L \cdot I_{CL}. \quad (7)$$

TABLE 1. The equations reformulated using normalized currents.

Equations reformulated using normalized currents
$I_{MC} = 1, I_{MP} = \gamma$ where $\gamma = I_{MP}/I_{MC}$
$I_{PC} = 1 - \xi_C$ where $\xi_C = I_{QC}/I_{MC} = I_{QC}$
$x_A = \xi_C/(1 - \xi_C)$
$I_C(\theta, x) = (1 - \xi_C) \cdot x \cdot \cos\theta + \xi_C, -\frac{\theta_{xC}}{2} < \theta < \frac{\theta_{xC}}{2}$
$I_{PP} = (1 + \xi_P) \cdot \gamma$ where $\xi_P = I_{QP}/I_{MP} = I_{QP}/\gamma$
$x_{break} = \xi_P/(1 + \xi_P)$
$I_P(\theta, x) = \gamma[(1 + \xi_P) \cdot x \cdot \cos\theta - \xi_P], -\frac{\theta_{xP}}{2} < \theta < \frac{\theta_{xP}}{2}$
Descriptions of parameters
γ: max. current ratio between carrier and peaking amplifiers
ξ_C: proportion of the quiescent current (carrier amp.)
ξ_P: proportion of the virtual quiescent current (peaking amp.)

Below the breakpoint ($0 \le x \le x_{break}$), as illustrated in Figure 5(a), only the carrier amplifier operates, satisfying the quarter-wave transformer relation as follows:

$$R_C = \frac{Z_0^2}{R_L}. \tag{8}$$

To maximize efficiency at the back-off power, the carrier amplifier should operate with its full voltage swing at the breakpoint, i.e.,

$$V_{C1}(x_{break}) = R_C \cdot I_{C1}(x_{break}) = V_{DD} - V_k \tag{9}$$

where V_{DD} and V_k are drain voltage and knee voltage, respectively.

Above the breakpoint ($x_{break} \le x \le x_{max}$), as illustrated in Figure 5(b), the peaking amplifier starts to operate and begins to modulate the load impedance. The quarter-wave transformer relation now becomes

$$R_C = \frac{Z_0^2}{R_{CL}}. \tag{10}$$

In this region, it is assumed that the carrier amplifier's output voltage $V_{C1}(x)$ remains constant at its maximum amplitude, i.e.,

$$V_{C1}(x) = V_{DD} - V_k. \tag{11}$$

From (7), (10), and (11), we can derive the relationship

$$I_{CL}(x) = \frac{V_{DD} - V_k}{Z_0}, \tag{12}$$

which implies that $I_{CL}(x)$ from the carrier amplifier reaches its highest value at the breakpoint and then remains constant throughout the high-power region above the breakpoint. To maximize the efficiency at the peak power, the voltage at the load (V_L) should fully swing:

$$V_L(x_{max}) = R_L[I_{CL}(x_{max}) + I_{P1}(x_{max})] = V_{DD} - V_k. \tag{13}$$

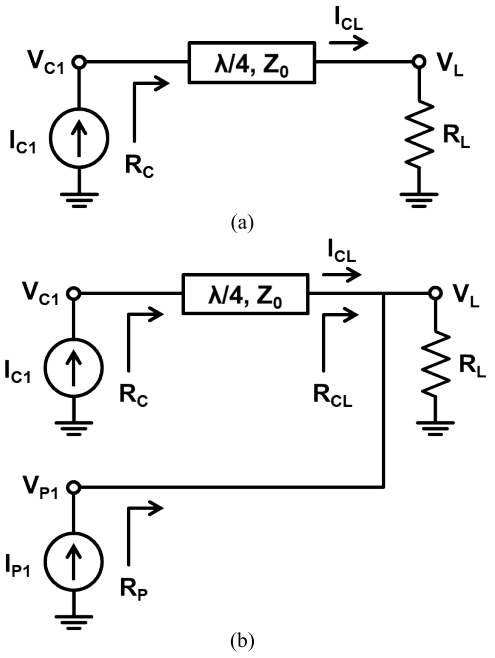

FIGURE 5. Equivalent Doherty circuit models: (a) below the breakpoint, (b) above the breakpoint.

Solving (8), (9), (12), and (13) simultaneously, we can determine the optimum values of R_L and Z_0. Then, we obtain output impedances, output voltage, output power, DC power consumption, and efficiency from the following relations:

output impedances

$$R_C = \frac{V_{C1}}{I_{C1}} = \begin{cases} \frac{V_{DD} - V_k}{I_{C1}(x_{break})} \text{ or } \frac{Z_0^2}{R_L}, & 0 \le x \le x_{break} \\ \frac{V_{DD} - V_k}{I_{C1}}, & x_{break} \le x \le x_{max} \end{cases} \tag{14}$$

$$R_P = \frac{V_L}{I_{P1}} = R_L\left(1 + \frac{I_{CL}}{I_{P1}}\right), x_{break} \le x \le x_{max} \tag{15}$$

output voltage

$$V_L = \begin{cases} R_L \cdot I_{CL} = \sqrt{R_L \cdot I_{C1} \cdot V_{C1}}, & 0 \le x \le x_{break} \\ R_L(I_{CL} + I_{P1}), & x_{break} \le x \le x_{max} \end{cases} \tag{16}$$

output power

$$P_{out} = \begin{cases} \frac{1}{2} V_L \cdot I_{CL} = \frac{1}{2} V_{C1} \cdot I_{C1}, & 0 \le x \le x_{break} \\ \frac{1}{2} V_L(I_{CL} + I_{P1}) = \frac{1}{2}(V_{C1} \cdot I_{C1} + V_L \cdot I_{P1}), & x_{break} \le x \le x_{max} \end{cases} \tag{17}$$

DC power consumption

$$P_{DC} = \begin{cases} V_{DD} \cdot I_{C0}, & 0 \le x \le x_{break} \\ V_{DD}(I_{C0} + I_{P0}), & x_{break} \le x \le x_{max} \end{cases} \tag{18}$$

efficiency

$$\eta = \frac{P_{out}}{P_{DC}}. \tag{19}$$

Since improved load modulation leads to higher efficiency, we can assess the effectiveness of the RUPS method by comparing it to the conventional methods. For comparison, we define four different cases of AB-C Doherty PAs as follows:

Case 1: The symmetric Doherty PA with EPS

Case 2: The asymmetric Doherty PA with EPS

Case 3: The asymmetric Doherty PA with RUPS, where the current of the carrier amplifier saturates after reaching its maximum current

Case 4: The asymmetric Doherty PA with RUPS, where the current of the carrier amplifier increases without saturation for the additional input drive

In Cases 3 and 4, the power splitting ratio is set to 1.5, indicating that the carrier amplifier receives 1.5 times more input power across the entire input power range. For the asymmetric configurations in Cases 2 and 3, the maximum current ratio between the two amplifiers is set to 1.5, implying that the peaking amplifier has a device periphery 1.5 times larger than that of the carrier amplifier. On the other hand, in Case 4, the peaking amplifier's maximum current is 1.5 times higher than the carrier amplifier's breakpoint current, suggesting that the carrier amplifier's current can increase after the breakpoint without saturation. Practically, this condition can be achieved by slightly increasing the size of the carrier device and adjusting the input matching network to ensure proper operation at the breakpoint, as mentioned earlier. To ensure a fair comparison, the output back-off range and the proportion of the quiescent current (ξ_C) of the carrier amplifier were uniformly set to 7.5 dB and 0.1, respectively, for all cases. For each case, the proportion of the virtual quiescent current (ξ_P) was optimized to achieve the back-off range of 7.5 dB. Consequently, when considering the asymmetric configurations, the values of ξ_P for Case 3 and 4 are 0.32 and 0.39, respectively, whereas the value of ξ_P for Case 2 is 0.48. This result indicates that the RUPS configurations operate in shallower class-C modes compared to the EPS case, as expected.

The fundamental and DC current profiles for each case are depicted in Figure 6. In Case 3 and 4, we observe that the current components of the carrier amplifier continue to increase until the peaking amplifier is fully utilized. In Case 3, the current slopes of the carrier amplifier start to decrease at a certain point in the high-power region due to current saturation. In Case 4, on the other hand, the current slopes of the carrier amplifier remain steady above the breakpoint as a result of mitigating current saturation. Furthermore, the impedance modulation profiles are depicted in Figure 7. While favorable modulation is observed in all cases, the Doherty PA in Case 4 exhibits the most appropriate load modulation.

The efficiencies for all the cases are depicted in Figure 8. The graph shows that the RUPS cases (Case 3 and 4) achieve better efficiencies than the conventional cases (Case 1 and 2) for most of the input drive range. When considering only the asymmetric cases, the RUPS Doherty PA shows an efficiency improvement of up to 2.4% compared to the EPS PA in the high-power region. The efficiencies of the RUPS Doherty

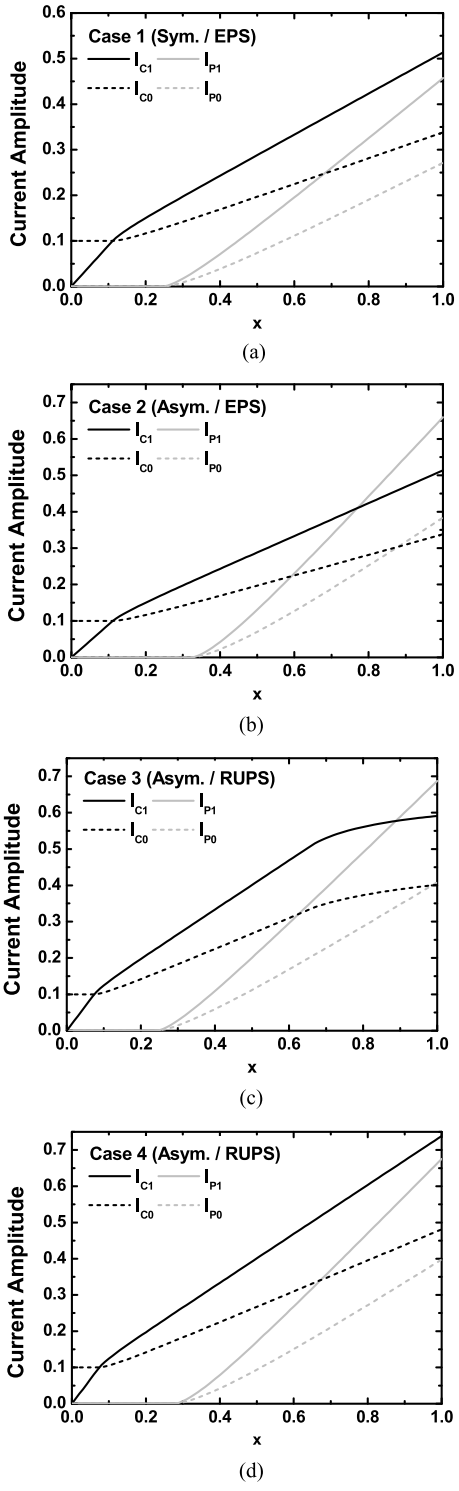

FIGURE 6. Fundamental and DC current profiles for four cases: (a) Case 1, (b) Case 2, (c) Case 3, (d) Case 4.

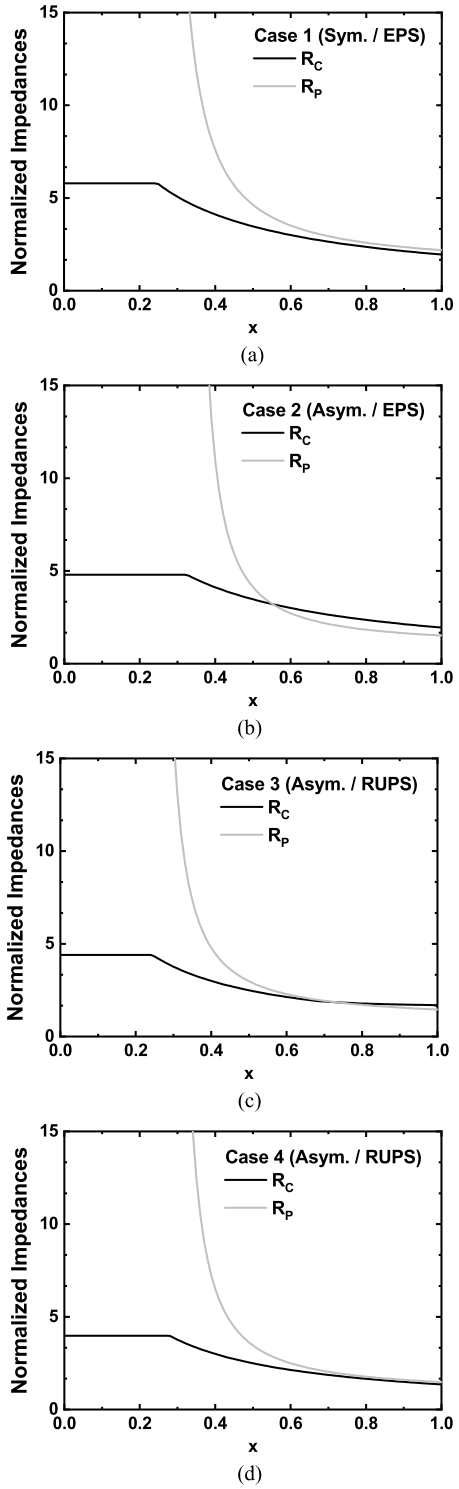

FIGURE 7. Normalized output impedances for four cases: (a) Case 1, (b) Case 2, (c) Case 3, (d) Case 4.

PAs exhibit significant improvements due to their shallow class-C operation and extended output power. Case 4 exhibits the highest efficiency across the entire power range among all the cases, thanks to its expanded operational power range.

We expect that the difference in efficiency becomes more significant in terms of PAE because the RUPS method can achieve higher gain than the conventional method due to the increased input drive and the shallow class-C operation of the peaking amplifier. The gain enhancement achieved by the RUPS method has been demonstrated in a previous study [23]. It should be noted that our analysis model primarily focuses on the output behavior, including output power back-off, output current, load modulation, and drain efficiency. Therefore, our model has limitations in capturing the PAE trend because it requires gain analysis based on the precise device models, which are not fully integrated into our analysis. Instead, in Section IV, we will validate the rationale behind the gain enhancement resulting from the RUPS method through experimental demonstration.

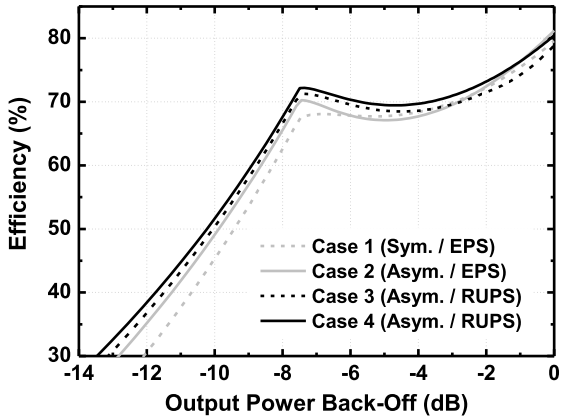

FIGURE 8. Efficiencies for the four cases as a function of x when the output back-off range is fixed to 7.5 dB.

Additionally, the RUPS configuration with a shallow class-C mode offers advantages in terms of linearity due to the reduced harmonic components of the peaking amplifier. A previous study [13] has effectively demonstrated the enhancement in linearity of an asymmetric Doherty PA through increased conduction angles. Furthermore, the increased gate bias voltage helps mitigate the electric field between the gate and drain, making the peaking amplifier less susceptible to breakdown.

III. GaN MMIC DOHERTY PAs WITH EPS AND RUPS CONFIGURATIONS

To demonstrate the effectiveness of the RUPS method with experimental investigations, we designed and fabricated Doherty PAs with the EPS and RUPS configurations. We employed GaN-based MMIC technology, which offers the advantage of compact size, making it suitable for use in a small-cell base-station PA for a 2.14-GHz long-term evolution (LTE) system.

A. DIRECTIONAL COUPLERS WITH EPS AND RUPS RATIOS

The power divider plays a critical role in implementing the power-splitting configurations. The four-port 90° hybrid directional coupler [26] is commonly used in Doherty PAs. The two output ports of the directional coupler have a phase

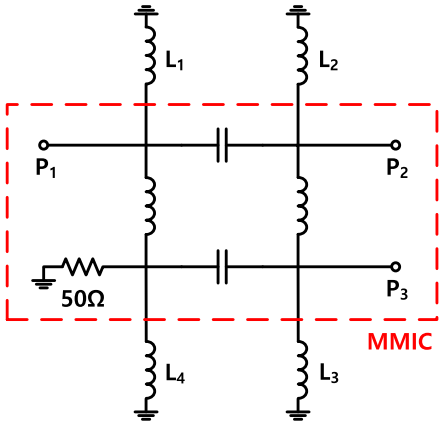

FIGURE 9. The schematic of the lumped-element directional coupler.

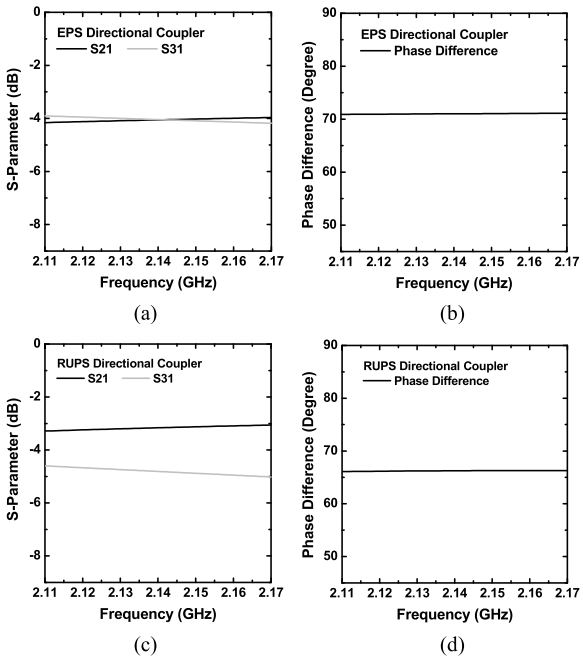

FIGURE 10. Simulated S-parameters and phase differences of the two types of directional couplers: (a), (b) EPS, (c), (d) RUPS.

difference of 90°, which can be utilized to cancel out the phase difference introduced by the impedance inverter. Alternatively, the three-port Wilkinson power divider [22], [26] is also widely used for the input splitting network, but it requires phase compensation as the two outputs are in-phase.

In this work, a lumped-element directional coupler [27] was utilized, as shown in Figure 9. The components within the dashed box were designed on the MMIC die, while the remaining components were implemented using off-chip components such as bonding wires, microstrip lines, and surface-mounted chip inductors. This approach was employed to minimize losses.

We designed two types of directional couplers with different power splitting ratios: the EPS and RUPS ratios. In the directional coupler with the RUPS ratio, the output port P_2, which supplies input power to the carrier amplifier, carries 1.5 times more power than port P_3, which is connected to the peaking amplifier. By modifying the external inductors ($L_1 \sim L_4$) of the directional coupler, the splitting ratio can be easily adjusted without requiring changes to the MMIC die layout. The splitting ratios were designed and optimized through electromagnetic simulation, and the results are presented in Figure 10. The S-parameters and phase differences at output ports P_2 and P_3 are shown as a function of frequency within the LTE band (2.11∼2.17 GHz), and key parameters at 2.14 GHz are summarized in Table 2. Both power splitting ratios were achieved using the same MMIC die, with very similar power losses. The phase differences deviate slightly from the typical value of 90° due to optimization to compensate for phase differences between the matching elements of the carrier and peaking amplifiers, as well as the impedance inverter. Additionally, a small variation in phase difference between the two power splitters was introduced during optimization to adjust the matching conditions.

TABLE 2. Simulation results of EPS and RUPS directional couplers.

Parameters @ 2.14 GHz	EPS Directional Coupler	RUPS Directional Coupler
S_{21}	-4.05 dB	-3.16 dB
S_{31}	-4.05 dB	-4.81 dB
Power Ratio (P_2 : P_3)	1 : 1	1.5 : 1
Total Power Loss	21%	19%
Phase Difference	71.0°	66.3°

B. DESIGN AND FABRICATION OF GaN MMIC DOHERTY PAs

The circuit schematic of the complete Doherty PA is shown in Figure 11. The design was based on the TriQuint 0.25-μm GaN HEMT 3MI process. To achieve an extended back-off range and proper load modulation, we employed an asymmetric configuration where the active device size of the peaking amplifier is 1.57 times larger than that of the carrier amplifier. The total gate widths of the carrier and peaking amplifiers are 2800 μm and 4400 μm, respectively. Lumped passive elements were utilized to design and implement key components such as the directional coupler, matching networks, and π-network impedance inverter, aiming to reduce the circuit size. More detailed design features have been described in the previous work [21].

A combination of an MMIC die and off-chip components provides a suitable compromise for achieving a small footprint and good efficiency. To effectively reduce size, key components including the input power splitter, matching networks, and impedance inverter were fabricated on the MMIC die, as indicated by the dashed box in Figure 11.

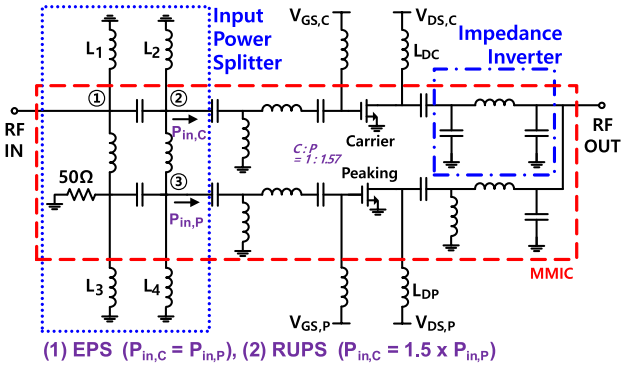

FIGURE 11. The schematic of the GaN MMIC Doherty PA.

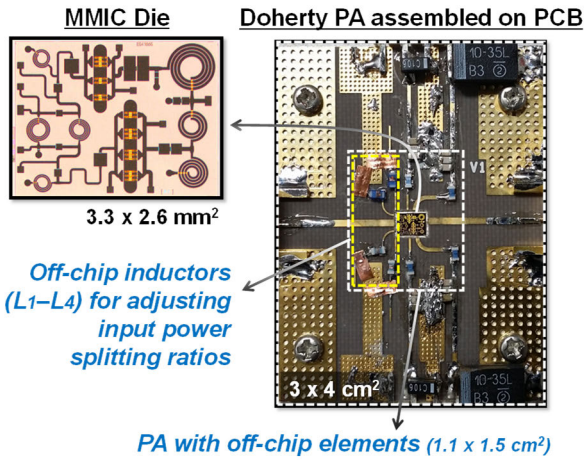

FIGURE 12. The photos of the fabricated GaN MMIC Doherty PA.

For the peripheral inductors located outside the box, high-Q surface-mounted chip inductors were used in conjunction with feeding lines and bond wires on a low-loss Taconic TLY printed circuit board (PCB) with a dielectric constant of 2.2. Photos of the fabricated MMIC and the assembled PA on the PCB are shown in Figure 12. The MMIC die (3.3×2.6 mm^2) and off-chip elements were assembled within an area of 1.1×1.5 cm^2, which is much smaller than a hybrid-type Doherty PA. The area can be further reduced by employing shorter feeding lines and smaller chip inductors.

IV. EXPERIMENTAL RESULTS

To demonstrate the performance of the RUPS GaN MMIC Doherty PA compared to the EPS configuration, we conducted a continuous-wave (CW) measurement at 2.14 GHz, which is the center frequency of an LTE downlink band (2110-2170 MHz), as shown in Figure 13. All amplifiers were operated with a drain bias voltage of 28 V. The gate bias voltages for the carrier amplifiers were set to −2.80 V for the EPS Doherty PA and −2.84 V for the RUPS Doherty PA. Although there was a slight variation in gate bias voltages, the quiescent currents of the carrier amplifiers were very similar, measuring 91 mA for the EPS Doherty PA and 90 mA for

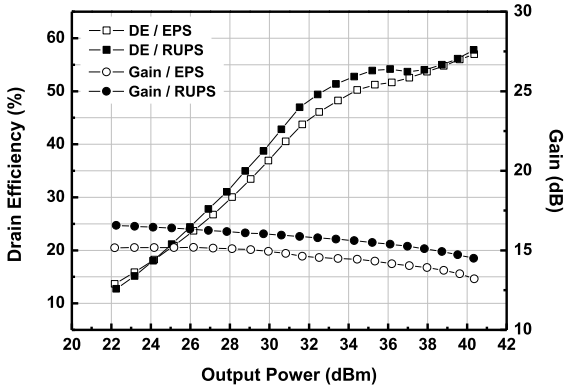

(a)

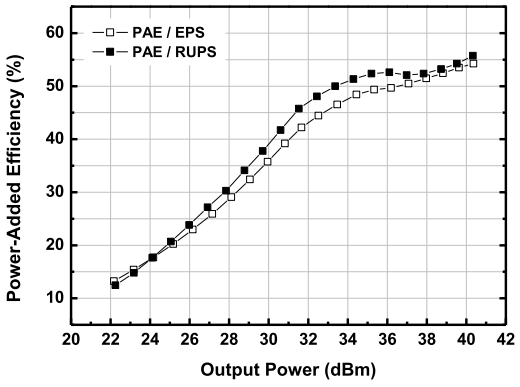

(b)

FIGURE 13. Measured CW characteristics of GaN MMIC Doherty PAs with the EPS and RUPS configurations: (a) DE, gain, (b) PAE.

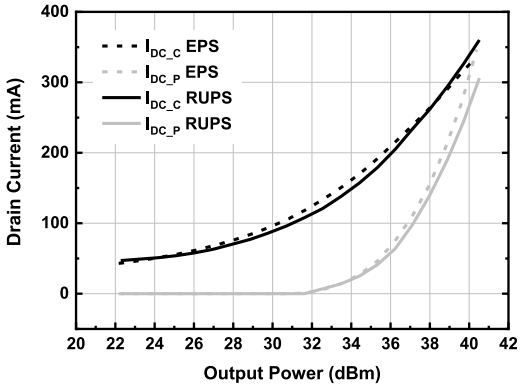

FIGURE 14. Measured DC currents versus output power of the EPS and RUPS Doherty PAs.

the RUPS Doherty PA. The peaking amplifier in the RUPS Doherty PA had a gate bias voltage of −3.66 V, while the EPS Doherty PA had a lower value of −4.29 V. This discrepancy in gate bias voltages confirms that the RUPS Doherty PA operates in a much shallower class-C mode, as explained in Section II.

As shown in Figure 13(a), the RUPS Doherty PA demonstrates a clear improvement in DE at various output powers, aligning with our earlier analysis. The observed difference in DE reaches up to 3.5%, exceeding the maximum difference

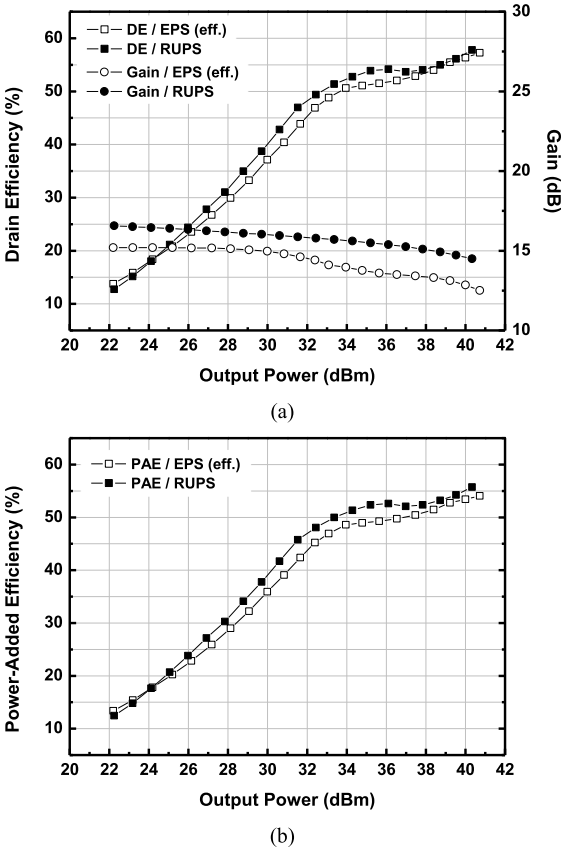

FIGURE 15. Measured CW characteristics of GaN MMIC Doherty PAs with the efficiency-enhanced EPS and RUPS configurations: (a) DE, gain, (b) PAE.

TABLE 3. Summary of measured performance using LTE signal.

Type	$V_{GS,P}$ (V)	$V_{GS,P}$ (V)	Gain (dB)	DE (%)	PAE (%)	ACLR (dBc)
EPS	-2.80	-4.29	14.5	47.7	46.1	-28.0
Efficiency -Enhanced EPS	-2.80	-4.56	14.1	48.6	46.7	-26.6
RUPS	-2.84	-3.66	15.7	51.8	50.4	-32.8

* The parameters were measured at an average power of 33.2 dBm
* Test signal: 2.14-GHz LTE signal with 10-MHz-bandwidth and 7.1-dB PAPR

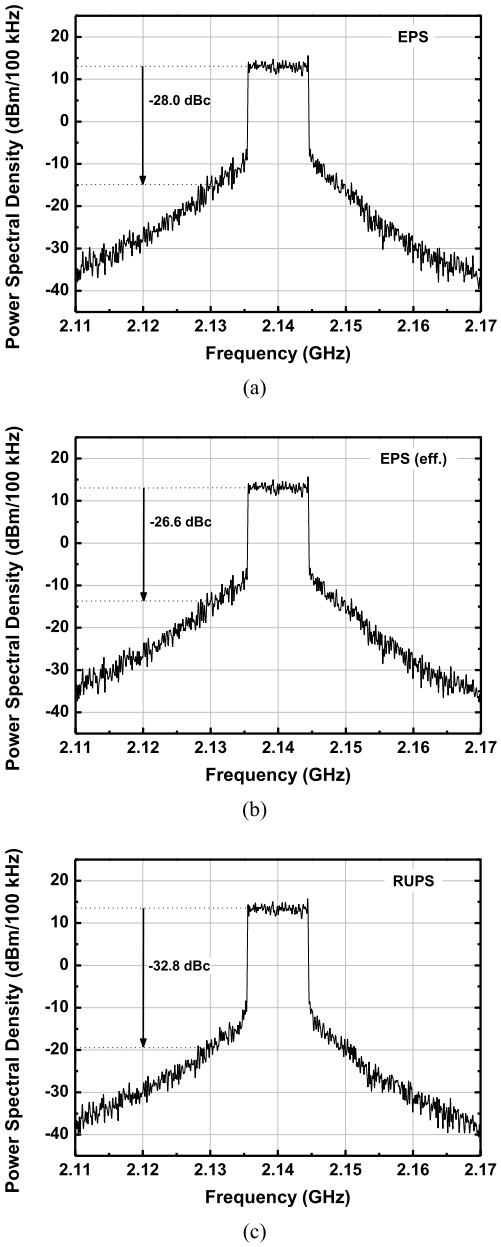

FIGURE 16. Measured 10-MHz-bandwidth LTE spectra for GaN MMIC Doherty PAs with (a) EPS, (b) efficiency-enhanced EPS, and (c) RUPS ratios, at an average output power of 33.2 dBm.

of 2.4% predicted in our analysis. This discrepancy between the analysis and measurement could be attributed to realistic factors that were not accounted for in the analysis.

The RUPS Doherty PA exhibits higher gains across the entire power range, with a gain enhancement ranging from 1.1 to 1.3 dB. As discussed in Section II, the gain improvement in the low-power region is attributed to the increased input power supplied to the carrier amplifier. In the high-power region, the gain is maintained with a consistent slope due to the shallower class-C operation. The gain enhancement leads to noticeable discrepancies in PAE, reaching up to 3.9% as shown in Figure 13(b).

The measured DC current profiles of both EPS and RUPS Doherty PAs are depicted in Figure 14. The input and output powers at the turn-on points are as follows: $P_{in} = 17.0$ dBm and $P_{out} = 31.7$ dBm for the EPS Doherty PA, while for the RUPS Doherty PA, they are $P_{in} = 15.8$ and $P_{out} = 31.6$ dBm. The shallow class-C operation causes the peaking amplifier of the RUPS Doherty PA to turn on at a lower input power compared to the EPS Doherty PA, which operates in a deep class-C mode. However, since RUPS delivers relatively less input power to the peaking amplifier, its turn-on output power is similar to that of the EPS Doherty PA. In summary, by employing RUPS, we can attain the benefits

TABLE 4. Performance comparison of fully-integrated GaN MMIC Doherty PAs (sub-6 GHz, single-stage).

Ref.	Freq. (GHz)	Symmetry	Input Power Splitting	Continuous Wave		Modulation Signal		
				DE (%) @ OBO[a]	Gain	DE [PAE] (%)	ACLR (dBc)[b]	PAPR
[14] 2015	2.1–2.7	A[c]	UPS	48.5–55[e] @ 7 dB	13–15[e]	46–53	-30 – -25[e]	7.2
[8] 2017	2.6	S[d]	EPS	54.2 @ 6 dB	13.7	54.4	-27.0	6.5
[15] 2018	4.3	A	EPS	44 @ 6 dB	15[e]	N/A	N/A	N/A
[9] 2019	3.3–3.8	S	EPS	42–51 @ 6 dB	12	N/A	N/A	N/A
[23] 2019	4.5–5.2	S	RUPS	47–50 @ 6 dB	8.6–11.6	43 @ 4.9 GHz	-29 @ 4.9 GHz	7.7
[10] 2019	4.5–6.0	S	EPS	24.4–31.6 @ 6 dB	7.6–11.6	[25.7] @ 5 GHz	-34 @ 5 GHz	8
[5] 2022	4.6–5.5	S	EPS	51–56.4 @ 6 dB	10.8–13	50–54	-25.4 – -22[e]	6.2
This Work	2.14	A	EPS	51.4 @ 6 dB[f] 50.3 @ 7 dB[f]	14.3 @ 6 dB 14.5 @ 7 dB	47.7 [46.1]	-28.0	7.1
			RUPS	54.2 @ 6 dB[f] 53.6 @ 7 dB[f]	15.4 @ 6 dB 15.5 @ 7 dB	51.8 [50.4]	-32.8	

[a]output power back-off, [b]w/o linearization, [c]Asymmetric, [d]Symmetric, [e]read from graph, [f]backed-off from 3-dB compression power

of gain enhancement in the low-power region and achieve efficient operation in the high-power region above the breakpoint through the shallow class-C operation of the peaking amplifier.

To assess the performance improvement in a general scenario, we compared the RUPS Doherty PA to an EPS Doherty PA with a different bias condition adjusted for higher efficiency. By adjusting the gate bias voltage of the peaking amplifier in the EPS Doherty PA from −4.29 V to −4.56 V, we achieved a deeper class-C operation, shifting the breakpoint to a higher output power. Consequently, the efficiencies improved at back-off output powers, as depicted in Figure 15. However, even with the deeper class-C operation, the RUPS Doherty PA still exhibited superior efficiencies.

The deeper class-C operation did improve the efficiency but had a detrimental effect on the gain, as shown in Figure 15(a). The gain begins to rapidly decrease around an output power of 33 dBm, and the amount of compression reaches 2.5 dB at 40.3 dBm. Therefore, it is evident that the deeper class-C operation induces significant gain compression in the high-power region, as discussed in Section II.

By observing the gain characteristics, we can make an estimation of the linearity. For example, the efficiency-enhanced EPS Doherty PA, despite its improved efficiency, may have poorer linearity due to substantial compression compared to the other PAs. However, when comparing the two gain curves in Figure 13(a), which exhibit similar compression behaviors, it becomes challenging to determine which one has better linearity. To evaluate linearity more clearly, we conducted measurements using a 2.14-GHz LTE modulated signal with a 10-MHz bandwidth and 7.1-dB PAPR. The power spectral densities were obtained at an output power of 33.2 dBm for all cases (EPS, efficiency-enhanced EPS, and RUPS), as depicted in Figure 16.

The RUPS Doherty PA demonstrates an adjacent channel leakage ratio (ACLR) of −32.8 dBc, while the EPS and efficiency-enhanced EPS Doherty PAs exhibit worse values of −28.0 dBc and −26.6 dBc, respectively. The linearity of the RUPS Doherty PA can be attributed to the reduction in harmonic components due to the shallow class-C operation of the peaking amplifier, as discussed in Section II. Additionally, it is worth noting that the efficiency-enhanced EPS Doherty PA exhibits a worse ACLR compared to the original EPS Doherty PA, as anticipated.

In terms of efficiencies and gain at average output power, the RUPS Doherty PA outperforms the EPS Doherty PAs. It achieves a DE of 51.8%, a PAE of 50.4%, and a gain of 15.7 dB. Compared to the EPS PA, the RUPS PA exhibits increments of 4.3% in PAE and 1.2 dB in gain. Similarly, when compared to the efficiency-enhanced EPS PA, the RUPS PA shows increments of 3.7% in PAE and 1.6 dB in gain. These results highlight the significant performance improvements achieved by the RUPS Doherty PA over conventional configurations. A summary of the measurement results can be found in Table 3. Furthermore, we compared the performance of our Doherty PA results with other single-stage GaN MMIC Doherty PAs and summarized them in Table 4. We observe that the RUPS Doherty PA demonstrates competitive efficiency at back-off power compared to other Doherty PAs, while also achieving excellent gain and linearity.

V. CONCLUSION

We investigated the effectiveness of the RUPS method for asymmetric Doherty configurations through numerical analysis and experimental demonstration. The RUPS Doherty PA, which involves supplying more input power to the carrier amplifier and operating the peaking amplifier in a shallow class-C mode, demonstrated substantial improvements compared to conventional EPS Doherty PAs. The fabricated RUPS Doherty PA, based on a 0.25-μm GaN HEMT MMIC process, achieved superior efficiency, gain, and linearity at 2.14 GHz. Specifically, for a 2.14-GHz CW signal, the PAE improved by up to 3.9%, and the gain increased by over 1 dB. When subjected to an LTE signal with a 7.1-dB PAPR, the RUPS Doherty PA demonstrated a 3.7–4.3% improvement in PAE and 1.2–1.6 dB higher gain compared to the conventional EPS PAs. Although the effectiveness of the

RUPS method was demonstrated using an asymmetric GaN MMIC Doherty PA in this study, it can be applied to generic asymmetric Doherty PAs, enabling significant performance enhancements.

REFERENCES

[1] V. Camarchia, P. Colantonio, F. Giannini, R. Giofrè, T. Jiang, M. Pirola, R. Quaglia, and C. Ramella, "A design strategy for AM/PM compensation in GaN Doherty power amplifiers," *IEEE Access*, vol. 5, pp. 22244–22251, 2017.

[2] R. Giofrè, P. Colantonio, and F. Giannini, "A design approach to maximize the efficiency vs. linearity trade-off in fixed and modulated load GaN power amplifiers," *IEEE Access*, vol. 6, pp. 9247–9255, 2018.

[3] A. Grebennikov and S. Bulja, "High-efficiency Doherty power amplifiers: Historical aspect and modern trends," *Proc. IEEE*, vol. 100, no. 12, pp. 3190–3219, Dec. 2012.

[4] G. Lv, W. Chen, X. Chen, F. M. Ghannouchi, and Z. Feng, "A fully integrated 47.6% fractional bandwidth GaN MMIC distributed efficient power amplifier with modified input matching and power splitting network," *IEEE Trans. Microw. Theory Techn.*, vol. 69, no. 6, pp. 3132–3145, Jun. 2021.

[5] R.-J. Liu, X.-W. Zhu, J. Xia, P. Chen, C. Yu, X.-L. Wu, and X. Chen, "Highly efficient wideband GaN MMIC Doherty power amplifier considering the output capacitor influence of the peaking transistor in Class-C operation," *IEEE Trans. Circuits Syst. I, Reg. Papers*, vol. 69, no. 5, pp. 1932–1942, May 2022.

[6] Y. Chen, W. Choi, J. Shin, H. Jeon, S. Bae, Y. C. Choi, S. Woo, Y. Y. Woo, H. Oh, K.-Y. Lee, K. C. Hwang, and Y. Yang, "Generalized expression and design method of modified load networks for Doherty power amplifier with extended back-off range," *IEEE Access*, vol. 10, pp. 77487–77497, 2022.

[7] K. Kwon, W. Choi, J. Shin, Y. Chen, Y. C. Choi, S. Bae, H. Jeon, J. Hwang, S. Woo, Y. Y. Woo, K.-Y. Lee, K. C. Hwang, and Y. Yang, "Compact load network having a controlled electrical length for Doherty power amplifier," *IEEE Access*, vol. 10, pp. 70440–70446, 2022.

[8] H. Lee, W. Lim, J. Bae, W. Lee, H. Kang, K. C. Hwang, K.-Y. Lee, C.-S. Park, and Y. Yang, "Highly efficient fully integrated GaN-HEMT Doherty power amplifier based on compact load network," *IEEE Trans. Microw. Theory Techn.*, vol. 65, no. 12, pp. 5203–5211, Dec. 2017.

[9] G. Lv, W. Chen, X. Liu, and Z. Feng, "A dual-band GaN MMIC power amplifier with hybrid operating modes for 5G application," *IEEE Microw. Wireless Compon. Lett.*, vol. 29, no. 3, pp. 228–230, Mar. 2019.

[10] G. Nikandish, R. B. Staszewski, and A. Zhu, "Bandwidth enhancement of GaN MMIC Doherty power amplifiers using broadband transformer-based load modulation network," *IEEE Access*, vol. 7, pp. 119844–119855, 2019.

[11] P. Colantonio, F. Giannini, and E. Limiti, *High Efficiency RF and Microwave Solid State Power Amplifiers*. Hoboken, NJ, USA: Wiley, 2009.

[12] M. Shahmoradi, S.-H. Javid-Hosseini, V. Nayyeri, R. Giofrè, and P. Colantonio, "A broadband Doherty power amplifier for sub-6GHz 5G applications," *IEEE Access*, vol. 11, pp. 28771–28780, 2023.

[13] J. Kim, B. Fehri, S. Boumaiza, and J. Wood, "Power efficiency and linearity enhancement using optimized asymmetrical Doherty power amplifiers," *IEEE Trans. Microw. Theory Techn.*, vol. 59, no. 2, pp. 425–434, Feb. 2011.

[14] S. Jee, J. Lee, J. Son, S. Kim, C. H. Kim, J. Moon, and B. Kim, "Asymmetric broadband Doherty power amplifier using GaN MMIC for femto-cell base-station," *IEEE Trans. Microw. Theory Techn.*, vol. 63, no. 9, pp. 2802–2810, Sep. 2015.

[15] R. Ishikawa, Y. Takayama, and K. Honjo, "Fully integrated asymmetric Doherty amplifier based on two-power-level impedance optimization," in *Proc. 13th Eur. Microw. Integr. Circuits Conf. (EuMIC)*, Sep. 2018, pp. 253–256.

[16] S. Park, H. Hwang, and S. Jeon, "An mm-wave multi-mode asymmetric power amplifier with back-off efficiency enhancement," *IEEE Access*, vol. 9, pp. 117282–117291, 2021.

[17] J. Guo, G. Crupi, and J. Cai, "A broadband asymmetric Doherty power amplifier design based on multiobjective Bayesian optimization: Theoretical and experimental validation," *IEEE Access*, vol. 10, pp. 89823–89834, 2022.

[18] J. Kim, J. Cha, I. Kim, and B. Kim, "Optimum operation of asymmetrical-cells-based linear Doherty power amplifiers-uneven power drive and power matching," *IEEE Trans. Microw. Theory Techn.*, vol. 53, no. 5, pp. 1802–1809, May 2005.

[19] D. Kang, J. Choi, D. Kim, and B. Kim, "Design of Doherty power amplifiers for handset applications," *IEEE Trans. Microw. Theory Techn.*, vol. 58, no. 8, pp. 2134–2142, Aug. 2010.

[20] M. Nick and A. Mortazawi, "Adaptive input-power distribution in Doherty power amplifiers for linearity and efficiency enhancement," *IEEE Trans. Microw. Theory Techn.*, vol. 58, no. 11, pp. 2764–2771, Nov. 2010.

[21] C. H. Kim, S. Jee, G.-D. Jo, K. Lee, and B. Kim, "A 2.14-GHz GaN MMIC Doherty power amplifier for small-cell base stations," *IEEE Microw. Wireless Compon. Lett.*, vol. 24, no. 4, pp. 263–265, Apr. 2014.

[22] C. H. Kim and B. Park, "Fully-integrated two-stage GaN MMIC Doherty power amplifier for LTE small cells," *IEEE Microw. Wireless Compon. Lett.*, vol. 26, no. 11, pp. 918–920, Nov. 2016.

[23] G. Lv, W. Chen, X. Liu, F. M. Ghannouchi, and Z. Feng, "A fully integrated C-band GaN MMIC Doherty power amplifier with high efficiency and compact size for 5G application," *IEEE Access*, vol. 7, pp. 71665–71674, 2019.

[24] A. M. E. Abounemra, W. Chen, F. Huang, M. Maktoomi, W. Zhang, M. Helaoui, and F. M. Ghannouchi, "Systematic design methodology of broadband Doherty amplifier using unified matching/combining networks with an application to GaN MMIC design," *IEEE Access*, vol. 9, pp. 5791–5805, 2021.

[25] S. C. Cripps, *RF Power Amplifiers for Wireless Communications*, 2nd, Ed. Norwood, MA, USA: Artech House, 2006.

[26] D. M. Pozar, *Microwave Engineering*, 4th ed. Hoboken, NJ, USA: Wiley, 2012.

[27] R. W. Vogel, "Analysis and design of lumped- and lumped-distributed-element directional couplers for MIC and MMIC applications," *IEEE Trans. Microw. Theory Techn.*, vol. 40, no. 2, pp. 253–262, Feb. 1992.

CHEOL HO KIM received the B.S., M.S., and Ph.D. degrees in electrical engineering from the Korea Advanced Institute of Science and Technology (KAIST), Daejeon, South Korea, in 2004, 2006, and 2012, respectively. He is currently a Senior Researcher with the Electronics and Telecommunications Research Institute (ETRI), South Korea. His research interests include both hardware and software fields, radio-frequency integrated circuits, power amplifiers, integrated device fabrication, reconfigurable antennas, artificial intelligence (AI), machine learning, deep learning, graphical models, and biologically inspired AI.

HYEON-JUNE KIM (Life Member, IEEE) received the B.S. degree from the Kumoh National Institute of Technology, Gumi, South Korea, in 2010, and the M.S. and Ph.D. degrees from the Korea Advanced Institute of Science and Technology, Daejeon, South Korea, in 2012 and 2017, respectively. In 2017, he joined SK Hynix, Icheon, South Korea, where he was worked on the product development of commercial CISs. From 2020 to 2023, he was with the Department of Electronics Engineering, Kangwon National University, Samcheok, South Korea, as an Assistant Professor. He has been with the Department of Semiconductor Engineering, Seoul National University of Science and Technology, Seoul, South Korea, since 2023, where he is currently an Assistant Professor. His current research interests include low-power mixed-signal ICs, RF ICs, CMOS image sensors, neuromorphic sensors, and object detection sensor systems.